ADVANCED FUNCTIONAL MATERIALS
www.afm-journal.de

Phase Transitions and Anisotropic Thermal Expansion in High Mobility Core-expanded Naphthalene Diimide Thin Film Transistors

*Eliot Gann, Xike Gao, Chong-an Di, and Christopher R. McNeill**

In situ grazing incidence wide-angle X-ray scattering (GIWAXS) is used to study the in situ thermal behavior of solution-processed, high mobility core-expanded naphthalene diimide thin films. A series of three different molecules is studied where the side-chain branching position is systematically varied through the use of 2-, 3- and 4-branched *N*-alkyl chains. For all molecules, a number of different phases and their associated phase transitions are observed with heating up to 200 °C. In situ GIWAXS measurements allow following significant variations of packing in each phase including crystalline coherence length, orientation, d-spacing, and paracrystallinity, as well as, for the first time, thin film thermal expansion coefficients in both the in-plane and out-of-plane direction. Relating these parameters with device measurements of quenched films, a striking correlation is found between high field-effect mobilities and low in-plane thermal expansion coefficients. This relationship indicates that high in-plane thermal expansion coefficients are detrimental to in-plane charge transport due to the formation of nanoscale defects in the critical first few monolayers upon quenching.

1. Introduction

Organic thin film transistors (OTFTs) are an important emerging technology with the promise of low cost and earth abundant constituent materials, facile large-scale fabrication from solution, and the ability to produce electronics on flexible and transparent substrates.[1,2] Side chains are a critical feature of the molecular structure of solution processable semiconductors often used in OTFTs. Although alkyl chains are not conductive, it is the solubilizing side chain which largely governs self-assembly while in solution, during the drying process, and again when annealed, which can beneficially arrange the rigid conjugated core of the molecules into crystalline domains that effectively transport charge across a device. Through judicious engineering of the molecular core, side chains, and solvent combinations, mobilities above 1 cm^2/Vs[2,3] have been achieved. However, there is little principled understanding of exactly what form of side chain is useful for producing a microstructure beneficial to high performance devices. There has been a significant amount of work recently investigating the effect of side chain length and branching position on the performance of completed devices.[4–6] However much of the success achieved has resulted from incremental alteration, not by principled design with mechanistic connections to performance. Because of the localized and anisotropic nature of the molecular orbitals in organic semiconductors, the exact orientation and spacing between planar aromatic elements can greatly affect charge mobility between molecules[7] and even subtle changes or defects in crystal structure can act as energetic barriers to charge transport.[8] Excess stress by side chain conformation and interaction can hinder beneficial molecular ordering, so the exact structure of side chains is important.[9] Often these effects can be empirically lessened and crystallinity can be increased by annealing the film, which allows long range restructuring and rearrangement of molecules into different phases.

The different crystalline forms of organic thin films have been extensively studied with the technique of grazing wide angle X-ray scattering (GIWAXS).[6,10–12] This technique allows films that are too thin for traditional X-ray or neutron crystallography to be probed by exploiting the great increase in X-ray field intensity when a highly collimated X-ray beam grazes a thin film near the film's X-ray critical angle, but below the critical angle of the substrate.[13] This geometry produces a

Dr. E. Gann
Australian Synchrotron
800 Blackburn Road, Clayton, VIC 3168, Australia
Dr. E. Gann, Prof. C. R. McNeill
Department of Materials Engineering
Monash University
Wellington Road, Clayton, VIC 3800, Australia
Dr. X. K. Gao
Laboratory of Materials Science
Shanghai Institute of Organic Chemistry
Chinese Academy of Sciences
Shanghai 200032, China
Dr. C.-A. Di
Beijing National Laboratory for Molecular Sciences
Key Laboratory of Organic Solids
Institute of Chemistry
Chinese Academy of Sciences
Beijing 100190, China
E-mail: christopher.mcneill@monash.edu

DOI: 10.1002/adfm.201401228

wave guiding effect within the film, greatly increasing the local X-ray electric field strength which in turn allows intensified scattering to be efficiently collected. This geometry limits GIWAXS to collecting only off-specular scattering and diffraction. The fixed incident angle that is employed disallows a traditional X-ray diffraction scan where the incident and measured angles and matched. Fortunately, the significant disorder in organic systems typically spreads the specular diffraction peaks well into the off specular plane, so that these peaks can still be well characterized despite not being fully captured.[14] A great benefit of this method is that both orientation and crystallinity are measured in a single exposure. Typical measures of organic thin films probed by GIWAXS include crystalline d-spacings, peak intensities, and peak widths in both orientational and radial directions. Simple peak widths can be used to determine a coherence length of the crystals, while a more complete peak shape analysis can further refine this coherence length, separating out the effects of paracrystallinity and crystallite size along different crystalline lattice directions.[14,15] In many thin film systems, and typical for conjugated polymers, a fully 3D crystalline diffraction pattern is not available, but only quasi liquid crystalline patterns with no or very weak mixed index peaks are apparent. GIWAXS is still highly useful in these cases, as lamella scattering peaks often match molecularly identifiable stacking directions, including the alkyl side chain packing direction and π-stacking direction, which often have strikingly different conduction properties. Careful measurement of these lamella peaks can be used to determine the orientation, order, coherence, and molecular tilt for these two important electronic directions.[10]

The efficiency of GIWAXS data collection, where often only a second or less is required for an exposure that allows the parameters listed above to be determined, opens up the possibility of collecting all the above parameters in an in situ experiment. In situ GIWAXS collection has been accomplished recently in the case of organic photovoltaic bulk heterojunction formation[16] and evolution upon annealing,[12] but has until now rarely been used to explore the in situ annealing of a small molecule OTFT thin films.[17] Monitoring the changing microstructure with respect to temperature in particular has the promise of elucidating the dynamics of system rearrangement, which can further guide developmental considerations in this emerging field.

In this work we employ in situ GIWAXS to study the evolution of high mobility core-expanded naphthalene diimide thin films with annealing. The molecules investigated are based on air-stable, solution-processable naphthalene diimides fused with 2-(1,3-dithiol-2-ylidene)malononitrile groups (NDI-DTYM2).[5] Recent work varying the alkyl branching position found that OTFT performance was optimised with the branching position located three carbon atoms from the conjugated core, with an electron mobility of 3.5 cm^2/Vs achieved.[5] For all molecules (with either a 2-, 3-, or 4-branching position) OTFT performance was found to be sensitive annealing of the active layer after solution deposition. For NDI2OD-DTYM2 (2OD) (with a branching position located 2 carbon atoms from the conjugated core of the molecule) OTFT mobility was observed to steadily increase from ≈0.05 cm^2/Vs for as-cast films, to ≈0.5 cm^2/Vs with annealing to 160 °C (and subsequently quenched). For NDI3HU-DTYM2 (3HU) (branching point located 3 carbon atoms from the core) mobilities of ≈0.04 cm^2/Vs were achieved with as-cast films increasing to up to 3.5 cm^2/Vs with annealing to 160 °C. Finally, for NDI4HD-DTYM2 (4HD) (branching point located 4 carbon atoms from the core) OTFT mobilities of 0.2 cm^2/Vs were observed in as-cast devices with mobility dramatically decreasing with annealing above 80 °C to a value of only 0.002 cm^2/Vs for a annealing temperature of 160 °C. Thus while the alkyl side chain branching position has been identified as a promising parameter for tuning of molecular structure of OTFT performance, the underlying link between side chain branching position and microstructural evolution is not well established.

The in situ GIWAXS measurements of NDI-DTYM2 thin films presented here provide new insight into the microstructural evolution of such films and the link between side chain branching position and OTFT performance. For each molecule we identify a number of different thin-film phases and characterise their associated in-plane and out-of-plane stacking parameters and phase transitions. In each of the phases of each of these materials, there is a strong peak in the out-of-plane direction which we attribute to lamella alkyl side chain stacking. For each phase of each molecule we determine the in-plane and out-of-plane thermal expansion coefficients often revealing a high degree of anisotropy in these parameters. Full crystalline unit cell parameters are not considered specifically in this analysis, but are provided for each identified phase in the Supporting Information. Significantly, we find a strong correlation between high OTFT mobilities with low in-plane thermal expansion coefficients, thus identifying the in-plane thermal expansion as an important parameter in determining the performance of thin film small molecule organic semiconductors.

2. Results

We first consider films of 2OD with a side chain branching location at the second carbon (**Figure 1**A). The in situ results upon heating are presented in Figure 1. Four unique but related phases are identified upon heating up to 200 °C. These structures, representative corrected GIWAXS patterns of which are shown in Figure 1 B, C, D, and E will be referred to respectively as 2OD-1, 2OD-2, 2OD-3, and 2OD-4. The first phase, 2OD-1, is present from room temperature up to 100 °C and shows a strong lamella stacking in the out-of-plane direction, corresponding to a d-spacing of 1.96(1) nm, a coherence length of 26(3) nm, a crystalline disorder parameter or paracrystallinity of 0.4(1)% and an orientation FWHM of 11.5 degrees. (All of these parameters are tabulated below in **Table 1**) In the in-plane direction, the dominant reflection corresponds to a d-spacing of 0.49 nm with a coherence length of 10 nm. This coherence length cannot be further reduced into the portion due to disorder (including paracrystallinity) and that due to crystalline size effects because we have only a single clear reflection and no indication that it is lamella in nature; however following the arguments made previously[18] the majority of the peak width is likely attributable to disorder rather than crystalline size effects. In general this phase shows a highly 3D crystallinity, with many mixed index peaks apparent. Between 100 °C and 125 °C, the

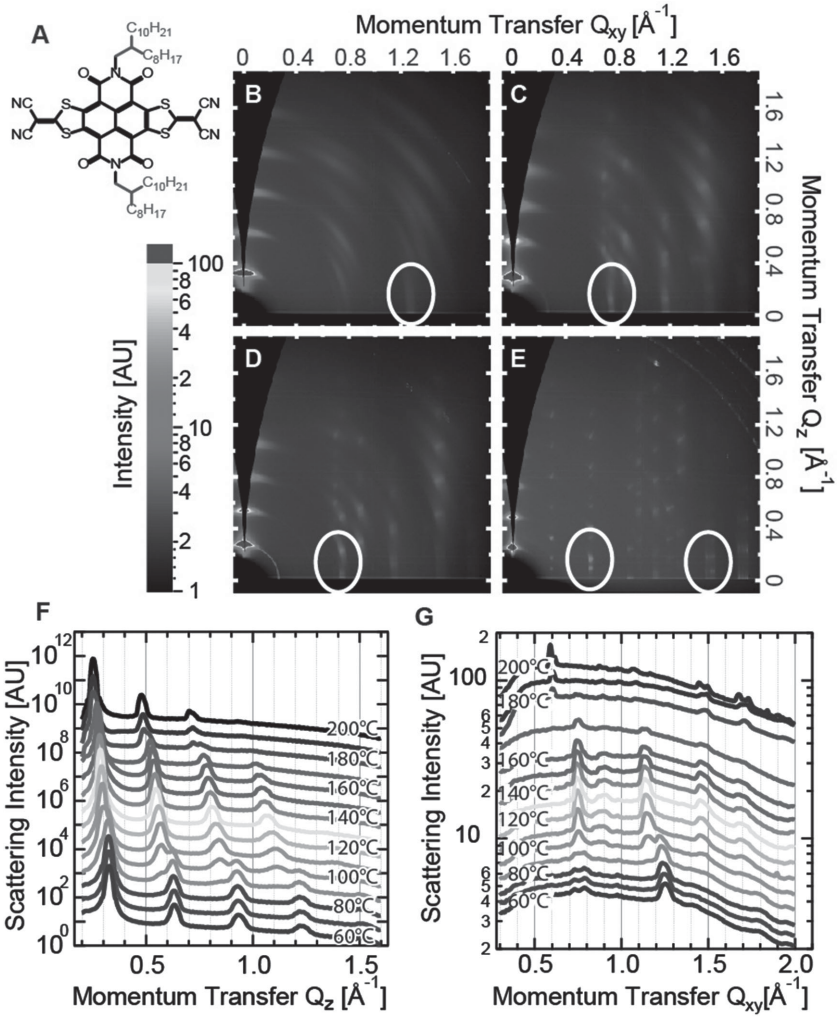

Figure 1. A) The chemical structure of 2OD. B–E) The Grazing incidence scattering pattern taken just about the critical angle of the different phases of 2OD. Taken at 30 °C, 110 °C, 140 °C, and 200 °C respectively. F) The out-of-plane scattering slice taken during a temperature ramp of 2OD thin film at 10 °C steps. G) The in-plane scattering slice taken during the same temperature ramp at the same temperatures. The traces in (F) and (G) are sequentially offset, by an exponential factor of 4 for each trace in F and 1.2 for each trace in G.

sample forms a second phase, 2OD-2. This narrow phase, only existing up to 125 °C, has an increased d-spacing in the out-of-plane direction of 2.15(1) nm, an increased coherence length of 32(2) nm, similarly small disorder of 0.4(1)% and a smaller orientational disorder of 9 degrees. In the plane of the film, the dominant spacing for 2OD-1 is 0.826(3) nm with a coherence length of 25(9) nm. From 125 °C through 180 °C a third phase, 2OD-3, appears, which is similar to 2OD-2 in spacings, but with a clearly different pattern of reflections in the off specular direction, perhaps indicating a similar crystalline structure but with a slightly differing confirmation with the substrate. 2OD-3 has a slightly increased out-of-plane lamella spacing of 2.28(2) nm with a similar coherence length of 33(6) nm and a tightened orientational width of 4.5 degrees. In the plane of the film, 2OD-3 has a dominant spacing at 0.83(1) nm and a much shorter coherence length of 8(5) nm. Finally above 180 °C, 2OD changes dramatically once again into a much more well-ordered phase, 2OD-4. The order can be seen in the dramatically reduced azimuthal peak width of 1.8 degrees. The spacing increases significantly to 2.60(1) nm, which is larger than the length of the molecule, indicating the unit cell contains at least two molecules shifted from each other vertically. The coherence length in the vertical direction is much larger, 45(2) nm, indicating much larger crystals, however the paracrystallinity remains at 0.5(1)%. In the plane of the film, the dominant spacing associated with this phase is 1.03(1) nm with a much larger coherence length of 39(5) nm. An additional in-plane peak at 0.409(2) nm and has a coherence of 20(6) nm. Figure 1F,G displays the out-of-plane and in-plane scattering cuts, respectively. Each cut is taken from the vertical or horizontal direction +/– 15 azimuthal degrees. Only one exposure for each 10 °C step between near room temperature to 200 °C is displayed for clarity, although intermediates were taken and utilized in results displayed below.

Although not of direct relevance to quenched samples, as measured previously and employed in OTFTs,[5] the stability of these phases was additionally probed by subsequently slow cooling samples down after reaching 160 °C and 200 °C, respectively. It was found that both of the corresponding phases at these temperatures, 2OD-3 and 2OD-4, were stable back to low temperature even at a relatively slow cooling rate, indicating that they are either energetic minima lower than that formed by spin coating (as seen in 2OD-1), or kinetically trapped states with long lifetimes through mechanisms such as side chain entanglement. The lower temperature phases, 2OD-1 and 2OD-2, were not cooled while taking exposures, so their stability was not measured.

Figure 2 presents the in situ GIWAXS results of thin films of the molecule 3HU, where the side chain branching position extended by an additional carbon atom (Figure 2A). Note that the branched side chains are also slightly shorter for 3HU (and 4HD) compared to NDI2OD-DTYM2. Upon heating to as much as 200 °C, 4 separate phases are identified, (Figure 2B–E) which will be referred to respectively as 3HU-1, 3HU-2, 3HU-3, and 3HU-4, each of which is considerably different than those found in 2OD.

The first phase present from room temperature up to 110 °C, 3HU-1, has a much smaller out-of-plane spacing (once again the alkyl side chain stacking direction) than any of those seen in 2OD-1, related to both the slightly shorter branched chains of NDI3HU-DTYM2, but in addition an overall tilting of the molecule or side chains in the unit cell. The out-of-plane lamella d-spacing is 1.62(2) nm with a coherence length of 40 nm and orientational width of 5 degrees. The lamella spacing of 3HU-1

Table 1. Thin film phases and morphological measures obtained by fitting GIWAXS line profiles of NDI-DTYM2 small molecules versus temperature.

Molecule-phase	Mobility	Crystal type	Minimum Temperature	Orientation disorder	Direction	d-Spacing	Coherence Length	Para-crystallinity	Peak Area	Thermal Expansion Coefficient
	[$cm^2 V^{-1} s^{-1}$]		[°C]	deg FWHM		[nm]	[nm]	[%]	AU	[$10^{-6} K^{-1}$]
2OD -1	0.05	3D	30	11.5	Out-of-plane	1.96 ± 0.01	26 ± 3	0.004 ± 0.001	10 000 ± 2000	500
					In-Plane	0.49 ± 0.01	10 ± 3	N/A	330 ± 150	350
2OD -2	0.2	3D	100	9	Out-of-plane	2.15 ± 0.01	32 ± 2	0.004 ± 0.001	30 000 ± 5000	500
					In-Plane	0.825 ± 0.003	25 ± 9	N/A	325 ± 100	20
2OD -3	0.5	3D	125	4.5	Out-of-plane	2.28 ± 0.02	33 ± 6	0.005 ± 0.001	22 000 ± 10 000	650
					In-Plane	0.83 ± 0.01	8 ± 8	N/A	310 ± 120	20
2OD -4	0.05	3D	180	1.8	Out-of-plane	2.6 ± 0.01	45 ± 2	0.005 ± 0.005	9000 ± 3000	500
					In-Plane	1.03 ± 0.01	39 ± 5	N/A	268 ± 50	150
					In-Plane	0.41 ± 0.005	20 ± 6	N/A	100 ± 40	300
3HU-1	0.04	3D	30	5	Out-of-plane	1.62 ± 0.01	40 ± 8	0.005 ± 0.005	30 000 ± 15 000	300
					In-Plane	0.492 ± 0.005	14 ± 3	N/A	500 ± 300	300
3HU-2	0.5	3D	100	1.1	Out-of-plane	2.2 ± 0.01	33 ± 4	0.007 ± 0.0005	26 000 ± 10 000	800
					In-Plane	0.71 ± 0.005	33 ± 7	N/A	650 ± 250	0
3HU-3	3.5	3D	120	2.1	Out-of-plane	2.29 ± 0.01	33 ± 6	0.0044 ± 0.0005	26 000 ± 1000	800
					In-Plane	0.79 ± 0.005	27 ± 8	N/A	500 ± 150	–50
3HU-4	0.5	LC	170	1.75	Out-of-plane	2.4 ± 0.07	42 ± 8	0.0047 ± 0.0001	8000 ± 3000	1500
					In-Plane	0.74 ± 0.01	21 ± 1	N/A	130 ± 20	–250
					In-Plane	0.364 ± 0.001	9 ± 1	N/A	100 ± 50	–50
4HD-1	0.2	3D	30	2.5	Out-of-plane	2.32 ± 0.05	37 ± 7	0.006 ± 0.0005	26 000 ± 10 000	550
					In-Plane	0.69 ± 0.01	22 ± 4	N/A	550 ± 300	100
					In-Plane	0.366 ± 0.001	2 ± 0.3	N/A	200 ± 100	200
4HD-2	0.005	LC	100	2.5	Out-of-plane	2.67 ± 0.03	35 ± 20	0.005 ± 0.001	15 000 ± 10 000	250
					In-Plane	0.86 ± 0.02	38 ± 2	N/A	450 ± 100	80
					In-Plane	0.4225 ± .001	16 ± 3	N/A	500 ± 300	350
4HD-3	0.001	3D	190	1.75	Out-of-plane	2.52 ± 0.01	33 ± 3	0.005 ± 0.001	10 000 ± 1000	N/A
					In-Plane	0.78 ± 0.01	25 ± 1	N/A	180 ± 50	N/A

has a slightly higher disorder parameter of 0.70(5)%. In the in-plane direction the dominant spacing is at 0.492(6) nm with a coherence length of 14(3) nm. Above 110 °C, the second phase, 3HU-2, is present only until 120 °C. In the out-of-plane direction, the lamella spacing increases dramatically to 2.20(5) nm with a coherence length of 33(6) nm and a much lower paracrystallinity parameter of 0.4(1)%. The orientational disorder of 3HU-2 is also significantly smaller than 3HU-1 at only 1.1(1) degrees. Above 120 °C there is a sudden phase change and a significant reduction in off specular peaks, indicating the 3D nature of the crystal is likely breaking down. Nevertheless, the lamella stacking in the out-of-plane direction stays largely the same, with a spacing of 2.292(2) nm, a coherence length of 33(6) nm and disorder of 0.5%. In the in-plane direction, however, 3HU-3 manifests a dominant in-plane peak at 0.794(6) nm with a coherence length of 27(8) nm. This phase also shows a slight widening of orientation disorder to a FWHM of 2.1 degrees. Finally above 170 °C, this phase melts gradually into the final phase 3HU-4, which displays only liquid crystalline order, with no mixed index peaks. The lamella stacking in the out-of-plane direction remains, with a d-spacing of 2.40(7) nm, coherence length of 43(8) nm and disorder of 0.6%. In the in-plane direction, several peaks are present, at 0.74(1) nm with a coherence length of 21(1) nm likely corresponding to stacking close to in the plane of the molecule and 0.365(2) nm with a coherence length of 9(1) nm, which because the morphology is liquid crystalline, we can relate to the π–π stacking distance common for π-conjugated molecules.[19] The orientation disorder of 3HU-4 is about the same as 3HU-3 at 1.75 degrees.

The vertical (out-of-plane) and horizontal (in-plane) azimuthal integrations for 3HU are shown in Figure 2F and 2G respectively, again only displaying a single trace for every 10 °C. We also explored the stability of these phases on slow cooling back to room temperature. We found that 3HU-3 remained upon slowly cooling down to 70 °C at which point, it reverted back to 3HU-1. 3HU-4, as it appeared as a relatively gradual liquid crystal melting of 3HU-3 reverted back reversibly into 3HU-3 by 170 °C upon cooling. The behavior of 3HU-2 on cooling was not explored, but because of the eventual reversibility of 3HU-3 and 3HU-4 into 3HU-1, it is likely also a

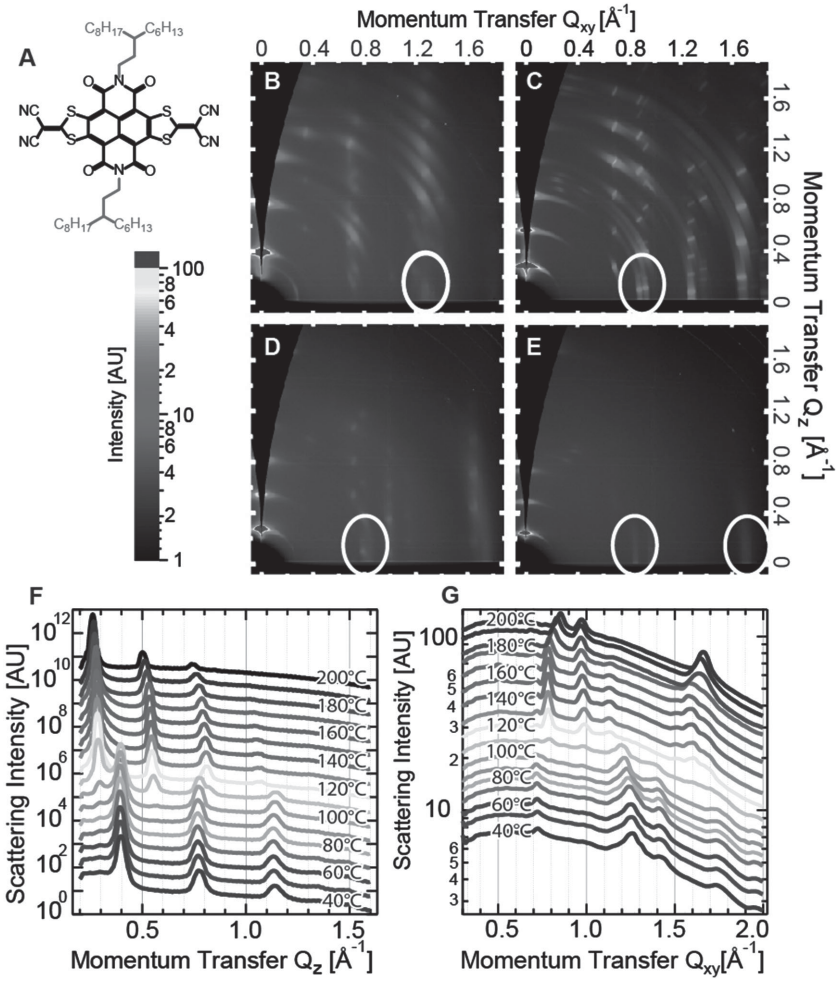

Figure 2. A) The chemical structure of 3HU. B–E) The Grazing incidence scattering pattern taken just about the critical angle of the different phases of 3HU. Taken at 30 °C, 110 °C, 150 °C, and 200 °C respectively. F) The out-of-plane scattering slice taken during a temperature ramp of 3HU thin film at 10 °C steps. G) The in-plane scattering slice taken during the same temperature ramp at the same temperatures. The traces in F and G are sequentially offset, by an exponential factor of 4 for each trace in F and 1.2 for each trace in G.

reversible transition. The reversibility of these transitions indicate that the phase changes of 3HU are not driven by finding successive energy minima unlocked by higher temperatures, but rather are more similar to first order phase transitions, unlocked when the system passes certain thresholds of free energy.

The final sample NDI4HD-DTYM2 (4HD) adds a single carbon before the branching point of the alkyl chains (**Figure 3**A), maintaining otherwise identical branch lengths to 3HU. This additional carbon changes the phase behavior of 4HD considerably. We only find 3 phases up to 200 °C and much longer gradual transitions than the relatively sudden transitions seen in both 2OD and 3HU. GIWAXS patterns from the three phases are shown in Figure 3B–D and will be respectively referred to as 4HD-1, 4HD-2, and 4HD-3.

The first phase of 4HD from casting at room temperature up to roughly 100 °C, 4HD-1, shows an out-of-plane alkyl stacking lamella spacing of 2.32(5) nm, a coherence length of 37(7) nm, and disorder of 0.5(1)%. In the in-plane direction, the dominant d-spacing is 0.69(1) nm with a coherence length of 22(4) nm. The orientation disorder in 4HD-1 phase is 2.5 degrees FWHM. The change from 4HD-1 to the more liquid crystalline 4HD-2 is gradual between 100 °C and 160 °C. 4HD-2 is characterized by a much larger alkyl stacking lamella distance of 2.67(3) nm with a coherence length of 35(10) nm and disorder again of 0.5(1)%. In the in-plane direction, there are again two major peaks, one at 0.860(2) nm with a coherence length of 38(2) nm, likely corresponding to the planar spacing of molecules in-plane, and one at 0.423(1) nm with a coherence length of 16(3) nm, which because of the liquid crystalline morphology we can once again relate to the π–π stacking direction. The larger alkyl stacking distance, as pointed out in the previous work[5] likely indicates a staggered pattern in-plane. The orientation disorder in this phase is again 2.5(1) degrees. At temperatures above 180 °C, we observe that the liquid crystal phase 4HD-2 changes further into another 3D crystal form 4HD-3. This 3D crystal has an intermediate alkyl stacking spacing of 2.52(1) nm and a coherence of 33(3) nm. In the out-of-plane direction, the dominant spacing is at 0.78(1) nm with a coherence of 25(1) nm and the orientational disorder of 4HD-3 decreases to 1.75 degrees FWHM.

Characterizing the stability of the 4HD phases upon cooling, we find that 4HD-2 returns partially to 4HD-1, although mixed phases are present even down below 60 °C. Upon reaching the 3D crystalline phase of 4HD-3, however, there is no transition back to 4HD-2, but there is again a partial transition back to 4HD-1 when reaching temperatures below 60 °C. It is difficult to characterize these phase transitions, as mixed phases are present at all temperatures, in stark contrast to the relatively quick transitions seen in both 2OD and 3HU. This may in part be the result of the branching location allowing long lived kinetic traps that hinder otherwise be energetically favorable phase transitions.

By creating automated routines to fit and classify peak groups, perform peak shape analysis, and plot the results of the analysis vs temperature and time, we follow the major reflections described above during temperature ramping, shown in **Figure 4**. We see that the different phases can often be identified, not only by d-spacing in plane and out of plane, but also by the thermal expansion, that is the slope of the d-spacing vs temperature line, normalized to the temperature at which the slope is measured.[20] From the slopes measured in Figure 4, along with inspection of peaks as shown in the lower portions of Figures 1–3, we define a morphological characteristic in addition to the spacing, direction, coherence, paracrystallinity,

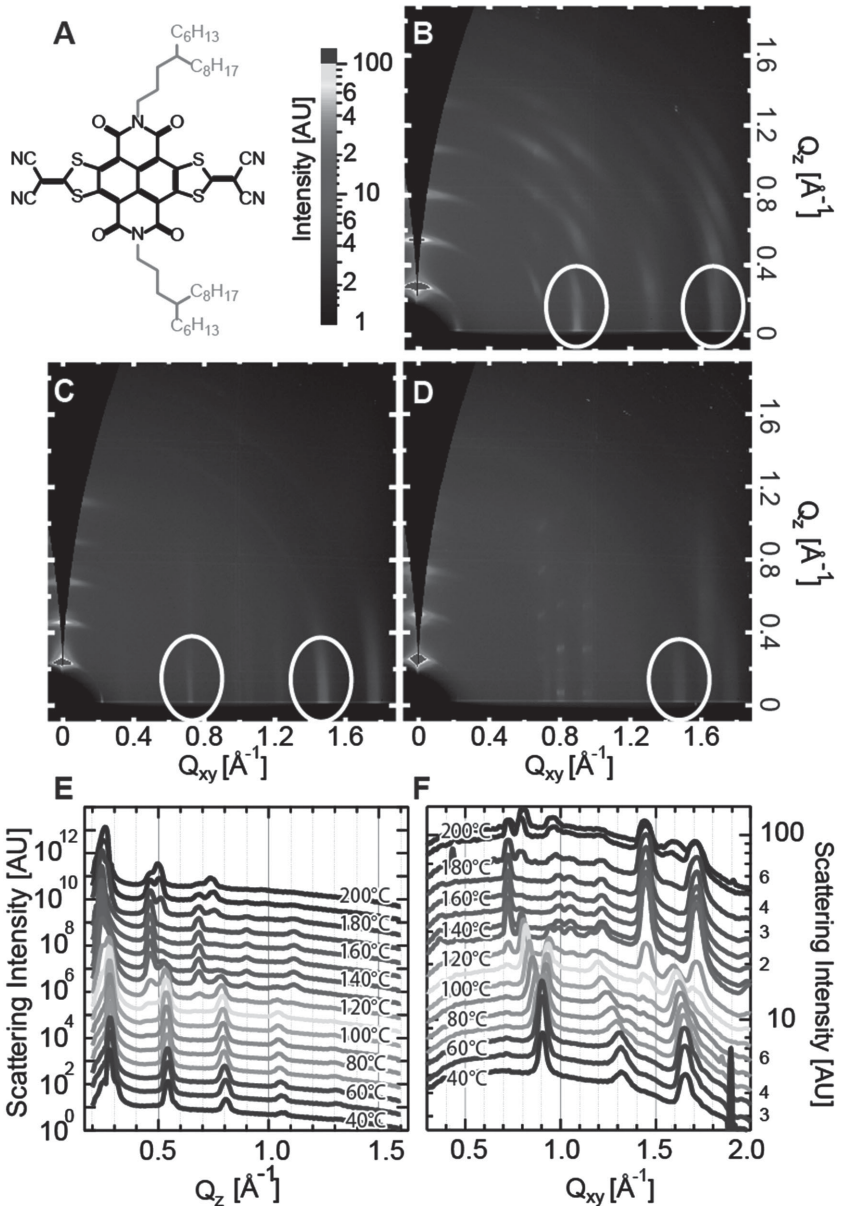

Figure 3. A) The chemical structure of4HD. B–D) The Grazing incidence scattering pattern taken just about the critical angle of the different phases of 4HD. Taken at 30 °C, 170 °C, and 200 °C respectively. E) The out-of-plane scattering slice taken during a temperature ramp of 4HD thin film at 10 °C steps. F) The in-plane scattering slice taken during the same temperature ramp at the same temperatures. The traces in E and F are sequentially offset, by a constant exponential factor of 4 for each trace in E and 1.2 for each trace in F. The jump in intensity near 130 °C and 190 °C are the result of different background level likely resulting from changing indices of refraction during phase transitions, or slight changes in incident angle.

and peak area we have already described for each phase. In most cases, the thermal expansion coefficients were taken during temperature ramp up, although it was found that the values of ramp down were similar, so ramp down values were used in the case of 2OD-4, 4HD-2, and 4HD-3 where the temperature range explored otherwise was too small to obtain reliable slope values. Additionally, mobility measurements of the quenched versions of these phases were taken from the previously published results, finding average mobility values for the temperature phase regions found here.[5] All of this data, as well as peak intensity are tabulated in Table 1.

3. Discussion

In the following we attempt to relate the microstructural parameters of the various phases to the corresponding OTFT mobilities. While OTFT data were taken of devices annealed to the specified temperature and then quenched, we argue that comparison of the in situ microstructural data with OTFT data is valid since the OTFT films were quenched following annealing at the specified temperature. Whatever crystal phase was created by annealing to that temperature will be preserved upon rapid quenching. Indeed, previous GIWAXS data taken of ex situ-prepared samples (annealed at 160 °C and then quenched)[5] match the crystalline forms that we measure here for in situ annealing at 160 °C (but with slightly different spacings due to thermal expansion).

A potential concern is that in most cases, only a single in-plane peak had low enough noise to clearly analyse. The previously measured unit cells[5] as well as the optimised unit cells shown in the Supporting Information are all close to orthorhombic and we find in all phases one axis identifiable as the alkyl side chain stacking direction highly aligned out-of-plane. We conclude this peak corresponds to a direction across the molecule from side chain to side chain because the unit cell sizes of about 2 nm match the molecular length across the alkyl side chains and there are often no other peaks which can contain the length of the molecule in this direction. We know it is lamella stacking because of the clear pattern of higher order reflections in an integer series. The remaining two unit cell axes are largely in the plane of the sample (see Supporting Information for optimized unit cell parameters). Thus only using one diffraction peak in the plane of the sample misses one of the unit cell dimensions. These axes however are difficult to identify molecularly, because it is highly unlikely that the molecule is oriented squarely in the unit cell, but can be twisted and tilted significantly.[5] This means that charge transport likely occurs along both in-plane unit cell directions. Additionally, the strong alkyl stacking and limited film thickness out-of-plane makes each plane a pseudo 2D system in which effects in an in-plane direction is closely coupled to other in-plane directions and less coupled to the out-of-plane direction. For all of these reasons, characterization of a single in-plane direction is valuable alone.

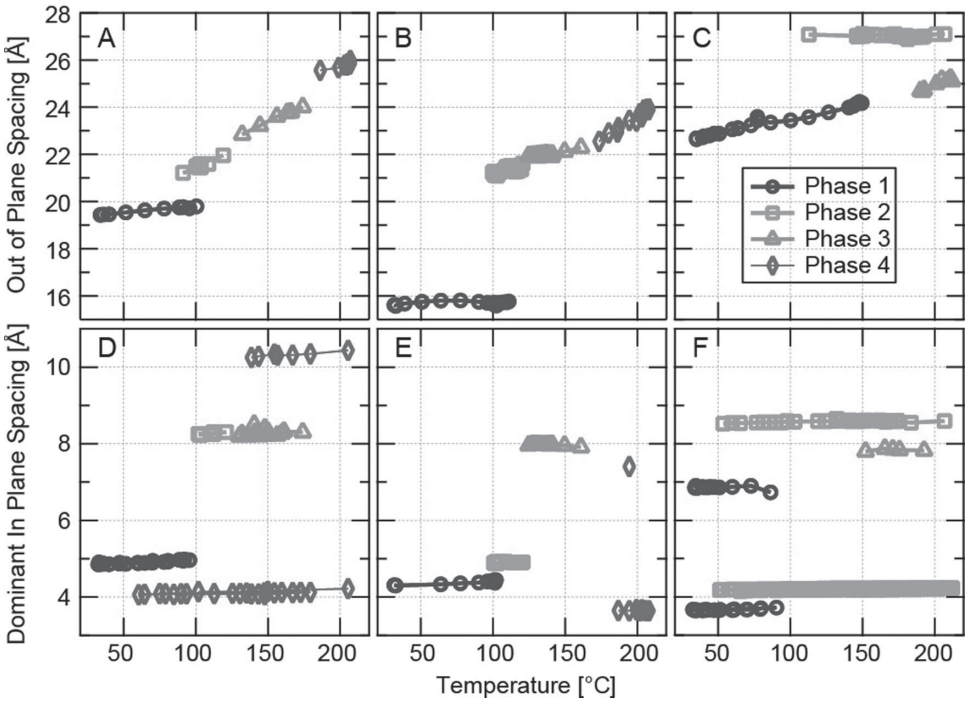

Figure 4. The dominant spacings for A–C) the out-of-plane scattering direction and D–F) the in-plane scattering direction. A,D) from 2OD. B,E) from 3HU. C,F) from 4HD. In all cases but C) phase 2, D) phase 4s, peaks are from an increasing temperature ramp. All peaks are found automatically by peak finding algorithms and split into phases by hand with the help of examination of the 2D scattering profiles from Figures 1–3. In addition to peak location, peak width, and area, in the out-of-plane peaks (A–C), crystalline disorder was fit simultaneously. A background function of a logarithmic cubic function was used to obtain all parameters.

To aid the interpretation of the results tabulated in Table 1, a statistical cross correlation test on all of these parameters was conducted, with the results shown in the cross-correlation plot of **Figure 5**A. Several interesting correlations are apparent. Strong correlation is seen between crystalline dimensions and temperature of the phase, particularly in the out-of-plane direction. This makes sense as the unit cell must in general expand with increasing free energy. Crystallinity (proportional to peak area and film thickness) is linked in all directions. This indicates that crystals generally grow and shrink in all dimensions simultaneously. Thermal expansion is correlated with lower crystallinity and increased disorder in crystals, which makes sense as crystals have to make long range rearrangements to conserve space as they are rapidly increasing or decreasing in size. Finally, orientational disorder is correlated with shorter coherence length and smaller crystals, as well as smaller d-spacings. This can be understood as larger crystals must have more widespread interaction with the substrate and so have increased pressure to align with the substrate and reduce orientational disorder.

As the performance measure of OTFTs, a detailed view of each parameter correlated with carrier mobility (measured previously as a function of annealing temperature[5] is shown as a bar graph in Figure 5B. It is important to note that all correlation coefficients are less than |0.6|, indicating no single measure completely decides performance in these materials. For many morphological characteristics, a lack of correlation in this dataset should not be taken to discount their importance to device performance in general, but rather to indicate that they are not bottlenecks to performance in this set of materials.

By far the parameters with the most effect on device performance, both positive and negative, are the thermal expansion coefficients, and most interestingly its impact is highly anisotropic. A larger thermal expansion in the out-of-plane direction has a positive correlation, while thermal expansion in-plane, particularly for the smaller spacings but in general for all spacings, appears detrimental. This differing behavior makes good sense, because of course the out-of-plane and in-plane coefficients of thermal expansion are related in these devices. Thermodynamics broadly drives a volumetric thermal expansion not each independent direction. If that volumetric expansion is taken up easily by out-of-plane expansion, it leaves the in-plane directions free to stay the same size, or even shrink slightly. Thus, the beneficial out-of-plane expansion can be understood just as a secondary measure of the detriment of in-plane thermal expansion. Quenching a sample with large in-plane thermal expansion, without giving it time or free energy for large scale reorganizations, can result in disorder and fracturing of crystals in the device-critical in-plane direction. Taking a nominal thermal expansion coefficient of a poorly performing phase of 0.003 K^{-1} and assuming this coefficient is constant from 200 °C down to 30 °C, a 50 nm crystal would contract approximately 2.5 nm. If each crystal did not fracture or change average location, but just contracted in place, this would result in a 2.5 nm gap between crystals. The substrate Si wafer under the same change in temperature contracts only 0.025 nm. The precise density of defects will depend on the

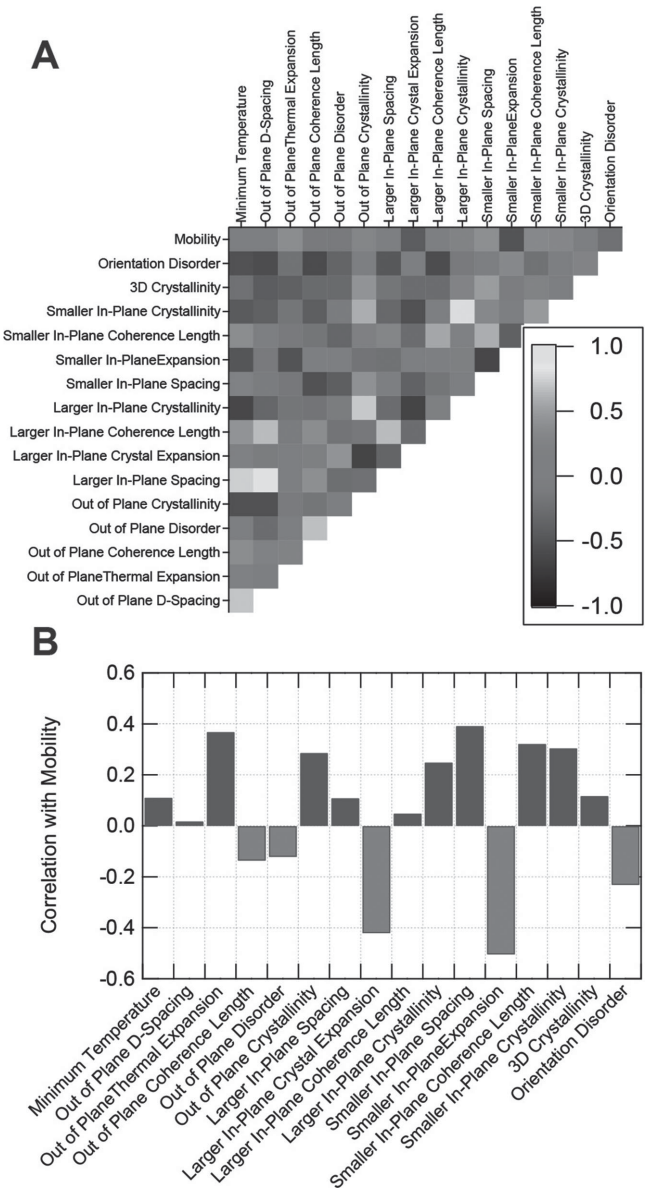

Figure 5. A) Cross correlation of morphological measures for all the crystalline phases shown in this paper. A value of 0 (red online) corresponds to no correlation, while 1 (yellow online) corresponds to perfect positive correlation and -1 (black online) corresponds to perfect negative correlation. B) The column of mobility is removed from A) and displayed as a bar graph to allow careful examination of performance correlations found in this set of samples.

friction of the substrate and upper layers, but a density on the level of the coherence length of the crystallites can explain the degraded performance, while being very difficult to characterize with a scanning probe technique. This is both because of the small defect size, but also because it is only the defects at the substrate layer which will directly affect device performance and the defects at the exposed surface may be significantly different.

The other largely detrimental parameter to mobility is orientational disorder. Because charge transport in OTFTs is generally confined to the first few layers, orientational disorder forces a 3D character to charge transport, which is not beneficial. Net positive correlations include crystallinity in all directions and coherence length in the in-plane directions, which together decrease the defect density a charge has to travel through. The correlation of increased in-plane crystalline spacing is likely a coincidence resulting from the selection bias of phases with a strong level of in-plane stacking. Finally, fully 3D crystals have a slight performance benefit over liquid crystalline phases, considered respectively as 1 and 0 for the correlation calculation.

We can further relate the anisotropic thermal expansion that is observed to be highly correlated with device performance back to the branching location of the carbon. Side chains are a natural location of thermal expansion, because of their ability to change conformation much more easily than the conjugated molecular core. Thus it is the behavior of the side chains upon heating which largely governs the thermal expansion within a phase. This set of samples reveals that each molecule has markedly differing phase and expansion behavior resulting from a subtle change in molecular structure. A branching location closer to the core allows thermal expansion in the vertical direction, perhaps indicating that the side chains are able to stay largely parallel in their crystalline form. For larger distances between the core and branching location, such as in 4HD, the side chains likely diverge into different directions to fill space more efficiently and thus expand and contract in multiple directions. The difference between 2OD and 3HU is a subtle one, but three carbons before the branching location in these samples seems to allow much more unidirectional expansion and contraction, whereas the 2-branching position allows slightly more expansion in-plane. For the optimum of 3 carbons before branching, an increasing temperature not only has a lengthening effect in the direction of the alkyl chains but additionally a shrinking effect in the other dimensions, allowing even closer packing in the critical in-plane direction at higher temperatures.

4. Conclusion

In situ GIWAXS measurements of NDI-DTYM2 thin films have revealed a rich phase behavior with each material studied exhibiting multiple thin-film phases. The pronounced differences in phase behavior between the 3 samples studied highlights the significant influence the alkyl chain branching position has on microstructural evolution. After characterising many parameters associated with each phase, we have identified a strong correlation between the measured in-plane thermal expansion co-efficient and the mobility of OTFT films that have been annealed and then quenched. Thus we highlight the in-plane thermal expansion co-efficient as a critically important parameter for solution-processed and thermally treated small molecule thin films, with tuning of the alkyl side chain branching position chains providing control over the anisotropic thermal expansion coefficients. The NDI-DTYM2 system allows an important isolation of this effect, revealing that in addition to the properties which have been established previously, thermal expansion is critical to consider in the further development of organic electronics.

5. Experimental Section

Details of material synthesis is provided in previous publications.[21] Films were prepared in an identical fashion to match our previous publication[5] by dissolving each material in chloroform at a concentration of 10 g/L and spin-coating at 2000 rpm. Trichloro(octadecyl)silane (OTS)-treated silicon wafers were used as substrates prepared as follows. Silicon wafers were first solvent cleaned in successive acetone and propan-2-ol solutions assisted by ultrasonication. The substrates were then cleaned by oxygen plasma treatment before being placed in a 10 mM solution of OTS in toluene at 60 °C for 20 min. The substrates were then successively rinsed with toluene and propan-2-ol before drying with nitrogen.

All data was collected at the small and wide angle X-ray scattering beamline at the Australian Synchrotron.[22] The collector was a Pilatus 1M active pixel detector with 0.172 mm × 0.172 mm pixels, in integration mode, positioned approximately 300 mm from the sample location. The sample was mounted in air on a heat stage, specially designed to allow grazing incidence measurements. Thermocouples mounted next to the samples allowed accurate temperature control. These molecules have been previously characterized to be stable in air to high temperature.[5] The precise sample-to-detector distance was determined with a silver behenate standard. 11 keV X-rays focused to approximately a 0.25 mm × 0.1 mm spot, was aligned at the critical angle of the sample by monitoring the direct beam with a diode while adjusting the angle of incidence. The close proximity of the diode to the sample allowed a simple alignment procedure of finding the maximum diode current, which would be just below the critical angle of the sample. A set of at least 10 exposures was taken at each temperature step to ensure that the critical angle did not change significantly and normalized data was collected. Data was reduced and analysed with a modified version of Nika.[23] GIWAXS patterns shown have been corrected onto to Qz and Qxy axes. Because of the fixed low incident angle necessary in GIWAXS, the resulting Q values in the vertical direction are a mixture of Qx (along the direction of the incoming X-rays) and Qz (normal to the surface or out-of-plane), which when corrected into 2D plots of Qz, and Qxy, results in the splitting of the data away from the Qz axis. For this reason, all of the 1D cuts shown were averaged sectors centerd at Qz ± 15 degrees. The Qz reflections are so intense, that even just catching the tails of the real peak is enough to well characterize several orders of reflections.

Supporting Information

Supporting Information is available from the Wiley Online Library or from the author.

Acknowledgements

This research was undertaken on the SAXS/WAXS beamline at the Australian Synchrotron, Victoria, Australia. We gratefully acknowledge the assistance of beamline scientists Nigel Kirby, Adrian Hawley, and Stephen Mudie. Additionally, we gratefully acknowledge Dr. Mark Styles (CSIRO, Division of Process Science and Engineering) who did the engineering design and construction of the in situ heater unit and its controls. This work was supported by the Australian Research Council (grant numbers FT100100275, DP130102616).

Received: April 17, 2014
Revised: June 11, 2014
Published online: September 11, 2014

[1] a) D. M. DeLongchamp, R. J. Kline, D. A. Fischer, L. J. Richter, M. F. Toney, *Adv. Mater.* **2011**, *23*, 319; b) R. A. Street, *Adv. Mater.* **2009**, *21*, 2007; c) J. Rivnay, L. H. Jimison, J. E. Northrup, M. F. Toney, R. Noriega, S. Lu, T. J. Marks, A. Facchetti, A. Salleo, *Nat. Mater.* **2009**, *8*, 952; d) C. Reese, M. Roberts, M.-M. Ling, Z. Bao, *Mater. Today* **2004**, *7*, 20; e) V. Coropceanu, J. Cornil, D. A. da Silva Filho, Y. Olivier, R. Silbey, J. L. Bredas, *Chem. Rev.* **2007**, *107*, 926.

[2] K. L. McCall, S. R. Rutter, E. L. Bone, N. D. Forrest, J. S. Bissett, J. D. E. Jones, M. J. Simms, A. J. Page, R. Fisher, B. A. Brown, S. D. Ogier, *Adv. Funct. Mater.* **2014**.

[3] J. Li, Y. Zhao, H. S. Tan, Y. Guo, C. A. Di, G. Yu, Y. Liu, M. Lin, S. H. Lim, Y. Zhou, H. Su, B. S. Ong, *Sci. Rep.* **2012**, *2*, 754.

[4] a) K. Balakrishnan, A. Datar, T. Naddo, J. Huang, R. Oitker, M. Yen, J. Zhao, L. Zang, *J. Am. Chem. Soc.* **2006**, *128*, 7390; b) P. F. Bazylewski, K. H. Kim, J. L. Forrest, H. Tada, D. H. Choi, G. S. Chang, *Chem. Phys. Lett.* **2011**, *508*, 90; c) X. R. Zhang, L. J. Richter, D. M. DeLongchamp, R. J. Kline, M. R. Hammond, I. McCulloch, M. Heeney, R. S. Ashraf, J. N. Smith, T. D. Anthopoulos, B. Schroeder, Y. H. Geerts, D. A. Fischer, M. F. Toney, *J. Am. Chem. Soc.* **2011**, *133*, 15073; d) J. Nelson, J. J. Kwiatkowski, J. Kirkpatrick, J. M. Frost, *Acc. Chem. Res.* **2009**, *42*, 1768; e) R. J. Kline, D. M. DeLongchamp, D. A. Fischer, E. K. Lin, L. J. Richter, M. L. Chabinyc, M. F. Toney, M. Heeney, I. McCulloch, *Macromolecules* **2007**, *40*, 7960.

[5] F. Zhang, Y. Hu, T. Schuettfort, C.-a. Di, X. Gao, C. R. McNeill, L. Thomsen, S. C. B. Mannsfeld, W. Yuan, H. Sirringhaus, D. Zhu, *J. Am. Chem. Soc.* **2013**, *135*, 2338.

[6] T. Schuettfort, S. Huettner, S. Lilliu, J. E. Macdonald, L. Thomsen, C. R. McNeill, *Macromolecules* **2011**, *44*, 1530.

[7] M. P. Samanta, W. Tian, S. Datta, J. I. Henderson, C. P. Kubiak, *Phys. Rev. B* **1996**, *53*, R7626.

[8] H. Sirringhaus, *Adv. Mater.* **2005**, *17*, 2411.

[9] A. Babel, S. A. Jenekhe, *Synth. Met.* **2005**, *148*, 169.

[10] P. Müller-Buschbaum, *Adv. Mater.* **2014**.

[11] a) H. G. O. Sandberg, G. L. Frey, M. N. Shkunov, H. Sirringhaus, R. H. Friend, M. M. Nielsen, C. Kumpf, *Langmuir* **2002**, *18*, 10176; b) C. He, D. S. Germack, R. Joseph Kline, D. M. Delongchamp, D. A. Fischer, C. R. Snyder, M. F. Toney, J. G. Kushmerick, L. J. Richter, *Sol. Energy Mater. Sol. Cells* **2011**, *95*, 1375; c) R. J. Kline, S. D. Hudson, X. R. Zhang, D. J. Gundlach, A. J. Moad, O. D. Jurchescu, T. N. Jackson, S. Subramanian, J. E. Anthony, M. F. Toney, L. J. Richter, *Chem. Mater.* **2011**, *23*, 1194; d) G. Renaud, R. Lazzari, F. Leroy, *Surf. Sci. Rep.* **2009**, *64*, 255; e) M. Y. Chiu, U. S. Jeng, C. H. Su, K. S. Liang, K. H. Wei, *Adv. Mater.* **2008**, *20*, 2573.

[12] N. D. Treat, C. G. Shuttle, M. F. Toney, C. J. Hawker, M. L. Chabinyc, *J. Mater. Chem.* **2011**, *21*, 15224.

[13] Z. Jiang, D. R. Lee, S. Narayanan, J. Wang, S. K. Sinha, *Phys. Rev. B* **2011**, *84*, 075440.

[14] J. Rivnay, R. Noriega, R. J. Kline, A. Salleo, M. F. Toney, *Phys. Rev. B* **2011**, *84*, 045203.

[15] B. E. Warren, B. L. Averbach, B. W. Roberts, *J. Appl. Phys.* **1951**, *22*, 1493.

[16] K. W. Chou, B. Yan, R. Li, E. Q. Li, K. Zhao, D. H. Anjum, S. Alvarez, R. Gassaway, A. Biocca, S. T. Thoroddsen, A. Hexemer, A. Amassian, *Adv. Mater.* **2013**, *25*, 1923.

[17] C. D. Liman, S. Choi, D. W. Breiby, J. E. Cochran, M. F. Toney, E. J. Kramer, M. L. Chabinyc, *J. Phys. Chem. B117*, 14557.

[18] J. Rivnay, R. Steyrleuthner, L. H. Jimison, A. Casadei, Z. H. Chen, M. F. Toney, A. Facchetti, D. Neher, A. Salleo, *Macromolecules* **2011**, *44*, 5246.

[19] I. McCulloch, M. Heeney, C. Bailey, K. Genevicius, I. MacDonald, M. Shkunov, D. Sparrowe, S. Tierney, R. Wagner, W. Zhang, M. L. Chabinyc, R. J. Kline, M. D. McGehee, M. F. Toney, *Nat. Mater.* **2006**, *5*, 328.

[20] a) D. Das, T. Jacobs, L. J. Barbour, *Nat. Mater.* **2010**, *9*, 36; b) P. P. Huo, P. Cebe, M. Capel, *J. Polym. Sci. Part B Polym. Phys.* **1992**, *30*, 1459.
[21] a) X. Gao, C.-a. Di, Y. Hu, X. Yang, H. Fan, F. Zhang, Y. Liu, H. Li, D. Zhu, *J. Am. Chem. Soc.* **2010**, *132*, 3697; b) Y. Hu, Y. Qin, X. Gao, F. Zhang, C.-a. Di, Z. Zhao, H. Li, D. Zhu, *Org. Lett.* **2011**, *14*, 292; c) Y. Hu, X. Gao, C.-a. Di, X. Yang, F. Zhang, Y. Liu, H. Li, D. Zhu, *Chem. Mater.* **2011**, *23*, 1204.
[22] N. M. Kirby, S. T. Mudie, A. M. Hawley, D. J. Cookson, H. D. T. Mertens, N. Cowieson, V. Samardzic-Boban, *J. Appl. Crystallogr.* **2013**, *46*, 1670.
[23] J. Ilavsky, *J. Appl. Crystallogr.* **2012**, *45*, 324.